Journal of Quantitative Spectroscopy & Radiative Transfer 158 (2015) 3–16

Contents lists available at ScienceDirect

Journal of Quantitative Spectroscopy & Radiative Transfer

journal homepage: www.elsevier.com/locate/jqsrt

Review

Implementation of optical dielectric metamaterials: A review

Shandra J. Corbitt, Mathieu Francoeur, Bart Raeymaekers *

Department of Mechanical Engineering, University of Utah, Salt Lake City, UT 84112, USA

ARTICLE INFO

Article history:
Received 18 September 2014
Received in revised form
29 October 2014
Accepted 8 December 2014
Available online 17 December 2014

Keywords:
Dielectric-based metamaterials
Manufacturing
Mie resonances
Optical response

ABSTRACT

Metamaterials are a class of man-made materials with exotic electromagnetic properties. The ability to fabricate three-dimensional macroscale metamaterials would enable embedding these structures in engineering applications and devices, to take advantage of their unique properties. This paper reviews the implementation of optical Mie resonance-based dielectric (MRD) metamaterials, as opposed to the more commonly used metallic-based metamaterials. Design constraints are derived based on Mie theory and related to fabrication specifications. Techniques to fabricate optical dielectric metamaterials are reviewed, including electron-beam lithography, focused ion beam lithography, nanoimprint lithography, and directed self-assembly. The limitations of each fabrication method are critically evaluated in light of the design constraints. The challenges that must be overcome to achieve fabrication and implementation of macro-scale three-dimensional MRD metamaterials are discussed.

Contents

1. Introduction

Electromagnetic metamaterials refer to a class of man-made materials consisting of sub-wavelength unit structures that display exotic properties such as negative magnetic

* Corresponding author. Tel.: +1 801 585 7594; fax: +1 801 585 9826.
E-mail address: bart.raeymaekers@utah.edu (B. Raeymaekers).

http://dx.doi.org/10.1016/j.jqsrt.2014.12.009
0022-4073/

permeability, negative electric permittivity and/or negative index of refraction [1–3]. The size of the unit structures, also referred to as "meta-atoms", is significantly smaller than the operating wavelength, but larger than the atomic and molecular structure [1]. The electromagnetic response of a metamaterial is the result of complex interactions between incident electromagnetic waves and the sub-wavelength unit structures, and can be predicted via a homogenization approach based on the effective electric permittivity and magnetic permeability. The possibility of tailoring the electromagnetic properties of a material by designing the unit structure of the meta-atoms has paved the way to conceptualizing many novel devices and technologies such as superlenses [4–8], hyperlenses [9,10], and optical cloaking [11–13]. Metamaterials also find application in nanoantennas [14,15], radiative cooling [16], thermal radiative property control [17–20] as well as in energy harvesting and conversion devices [21,22] to only name a few.

Most metamaterials operating in the optical frequency band that are documented in the literature are made of metallic meta-atoms such as split-ring resonators, thin wires, rods or fishnet structures [1,23]. They require two types of meta-atoms to induce both electric and magnetic responses. For instance, split-ring resonators are employed for tailoring the effective permeability while wires enable control of the effective permittivity [24], thus offering flexibility to the metamaterial designer. However, metallic metamaterials also present several drawbacks. Fabrication of the intricate structures that form the meta-atoms typically requires sophisticated micromanufacturing techniques, which are time consuming and not easily scalable to manufacture macroscale three-dimensional (3D) specimens that can be integrated in engineering devices [25]. Additionally, large ohmic losses exist, and the effective electromagnetic response of the metamaterial is anisotropic as a result of the asymmetric geometry of the metallic split-ring and wire inclusions.

In contrast, Mie resonance-based dielectric (MRD) metamaterials consist of dielectric meta-atoms, such as spherical, cylindrical, or randomly shaped inclusions embedded in a dielectric host medium. The electric and magnetic resonances of the inclusions are the building blocks that dictate the effective electromagnetic properties of the metamaterial. Mie theory offers an exact solution of Maxwell's equations for electromagnetic wave scattering and absorption by a single spherical particle [26]. The term "Mie" is loosely used for MRD metamaterials to specify that the effective electromagnetic response of the metamaterial depends on the electric and magnetic resonances of the dielectric inclusions. However, these dielectric inclusions are not restricted to spheres and may take various shapes.

MRD metamaterials present potential advantages compared to metallic metamaterials. Since the electromagnetic response of MRD metamaterials relies on the electric and magnetic resonances of dielectric inclusions, only one type of inclusion can be used to induce both effective electric and magnetic resonances. Additionally, an isotropic electromagnetic response can be obtained with spherical inclusions or by using a large amount of randomly oriented, non-symmetric inclusions [27]. Losses for MRD metamaterials are expected to be smaller than for metallic metamaterials [25].

The electromagnetic response of MRD metamaterials can be engineered by varying the host medium and the shape, shape distribution, material, size, size distribution, spatial arrangement or concentration of the dielectric inclusions. The spatial arrangement of the inclusions can be adjusted from randomly dispersed to periodic, since the effective properties rely on the resonances of the dielectric inclusions, not the periodicity of the arrangement [1]. As a result, the role of fabrication imperfections in MRD metamaterials is less important than in the case of metallic metamaterials, where alignment and periodicity of the features is critical to obtaining the desired response.

MRD metamaterials operating in the microwave spectral band have been experimentally studied over the past few years [28–32]. The size of the inclusions and their separation distance can be as large as a few millimeters and, thus, fabrication is less challenging and can be accomplished with traditional, macroscale techniques. This review focuses on MRD metamaterials operating at optical wavelengths, which covers both the visible and the infrared spectral bands. Although several optical MRD metamaterials have been developed theoretically [33–42], few authors provide detailed information about possible fabrication methods, and even fewer published works documenting successful fabrication and implementation of optical MRD metamaterials [27,43–48]. In addition, the specimens fabricated in these studies are typically microscale two-dimensional (2D) specimens, with restrictions on the orientation of incident waves. Thus, they cannot easily be used in macroscale engineering applications. To take advantage of the exotic electromagnetic properties of MRD metamaterials in engineering systems and applications, fabrication of 3D macroscale metamaterial specimens is imperative. Hence, high-precision, high-throughput, and low-cost scalable manufacturing processes are needed to fabricate macroscale 3D MRD structures operating at optical frequencies. Furthermore, integration between metamaterial design and fabrication is critical to successfully implementing macrosale MRD metamaterials. Thus, the objective of this review is two-fold. First, we establish the design and fabrication requirements needed to implement MRD metamaterials. Second, we review the manufacturing techniques that have been reported in the literature to successfully fabricate a proof-of-concept of all-dielectric optical metamaterials. Additionally, we discuss fabrication techniques that have been proposed, or are viable in principle, but have not yet been successfully implemented for MRD metamaterials. We point out that a review of fabrication techniques for metallic-based metamaterials has been provided by Boltasseva and Shalaev [23].

2. Design and fabrication requirements for engineering electric and magnetic resonances with MRD metamaterials

The effective electromagnetic response of MRD metamaterials depends on the interplay between the dielectric inclusions and the host medium, and can be engineered by

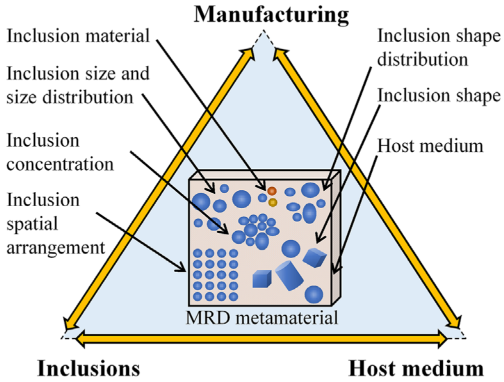

Fig. 1. Adjustable parameters affecting the effective electromagnetic response of an MRD metamaterial.

means of the adjustable parameters graphically summarized in Fig. 1. These include the host medium material, and the shape, shape distribution, material, size, size distribution, spatial arrangement and concentration of inclusions. The manufacturing technique is often a limiting factor in terms of the different designs that can be achieved.

In addition, other requirements must be satisfied to implement a functional MRD metamaterial in engineering devices. First, the "meta-atomic" structure must be 3D to ensure an isotropic electromagnetic response from the MRD metamaterial. For instance, a patterned surface is a 2D structure leading to anisotropic effective electromagnetic properties. Second, the size of the 3D meta-atoms must be smaller than the wavelength of the electromagnetic wave. This implies that the size of the inclusions in the three coordinate directions must not exceed a few tens of nanometers for metamaterials operating in the visible spectral band, and not exceed a few micrometers for metamaterials operating in the infrared band. Additionally, the size of the fabricated specimens must at least measure several millimeters in the three coordinate directions to be embedded in engineering devices.

Appendix A presents a detailed discussion of the effective electric and magnetic resonances in MRD metamaterials. Dielectric inclusions exhibiting both electric and magnetic dipolar resonances are required to engineer the effective electromagnetic response of an MRD metamaterial. Hence, this design requirement limits the materials that can be used as inclusions. From the discussion in Appendix A, electric dipole resonance can be achieved via inclusions with large electric permittivity relative to the host medium permittivity and/or negative electric permittivity, while magnetic dipole resonance requires inclusions with large electric permittivity. At optical frequencies, polaritonic materials such as silicon carbide (SiC), quartz, cubic boron nitride, doped silicon [49] and materials exhibiting low loss and moderate permittivity such as silicon (Si), germanium (Ge), tellurium (Te), titanium dioxide (TiO_2) and silica [45–48,50–52] fulfill these requirements.

Minimizing losses in metamaterials is important especially when dealing with 3D macroscale specimens. Metamaterial losses can be quantified using the figure of merit (FOM) defined as $|\mathrm{Re}(n)/\mathrm{Im}(n)|$, where n is the refractive index [25]. Physically, the FOM is an indicator of the wave amplitude decay over a length of one medium wavelength calculated as $\exp(-2\pi/\mathrm{FOM})$. Metallic-based metamaterials suffer from large losses and a FOM of 3 is the largest measured value reported in the literature [53,54]. MRD metamaterials should in theory have a higher FOM than metallic metamaterials, but no experimental evidence has been reported thus far. Polaritonic materials with large permittivity exhibit significant losses near the resonance frequency, as illustrated in Fig. A1.1 for the case of SiC. As such, polaritonic inclusions may not be ideal for improving the FOM [45]. Inclusions made of materials such as Si or Ge are better candidates for maximizing the FOM as the real part of their refractive index is moderately high ($\sim$3.5 for Si and $\sim$4 for Ge) in the near infrared where losses are essentially negligible [45,52,55]. However, a need still exists to experimentally demonstrate that a large FOM can be obtained with MRD metamaterials made of quasi-lossless inclusions.

A single type of dielectric inclusions is sufficient to induce effective electric and magnetic responses in MRD metamaterials. On the other hand, realization of an MRD metamaterial with negative refractive index is not as straightforward, because it requires spectrally overlapping electric and magnetic dipole resonances. Various approaches have been proposed to induce overlapping electric and magnetic resonances in MRD metamaterials. Zhao et al. [24] theoretically demonstrated that negative refraction can be engineered in MRD metamaterials using coated spheres, where the core and the shell induce overlapping electric and magnetic dipole resonances. Wheeler et al. [56] analyzed an MRD metamaterial made of spheres with a lithium tantalate ($LiTaO_3$) core coated with a semiconductor having an electromagnetic response described by a Drude model. The metamaterial resulted in negative refraction in the infrared spectral band. Alternatively, two sets of inclusions of the same materials but with different sizes can generate spectrally overlapping electric and magnetic dipolar resonances, thus leading to negative refraction [35]. Yannopapas [37] theoretically demonstrated that negative refraction is achievable in the infrared band with a mixture of $LiTaO_3$ and n-type Ge spheres. A different approach is based on embedding dielectric inclusions with magnetic dipolar resonance in a host medium exhibiting negative permittivity [25,36,38,57]. For example, Kussow et al. [36] showed isotropic negative refraction in the visible spectrum in an MRD metamaterial consisting of SiC spherical inclusions embedded in a polycrystalline magnesium diboride (MgB_2) matrix. Wang et al. [29] demonstrated negative refraction in an MRD metamaterial at microwave frequencies using a single type and size of rectangular resonators that possesses simultaneous electric and magnetic responses. They pointed out that such structure can also be realized at optical frequencies. Recently, Staude et al. [46] experimentally demonstrated spectrally overlapping electric and magnetic dipole resonances in the near infrared via a metamaterial made of a 2D periodic array of Si nanosize cylinders embedded into a low refractive index medium. Spectrally overlapping electric and magnetic resonances were achieved by varying the cylinder aspect ratio.

Furthermore, no design nor fabrication constraint is associated with the shape and the spatial arrangement of the dielectric inclusions. Various shapes such as spheres, cylinders, cubes or ellipsoids can be employed as inclusions for MRD metamaterials. The resonant modes of an inclusion are a function of its geometry, such that the inclusion shape influences the overall effective electromagnetic response of MRD metamaterials [24]. Although periodic patterns of dielectric inclusions are not required to obtain an MRD metamaterial, most demonstrations attempt to implement periodic structures to obtain better control of the optical response of the metamaterial, thus simplifying the comparison against theoretical predictions. Hence, the spatial arrangement of inclusions is used as an adjustable parameter to tune the optical response of the metamaterial, not a required parameter as is the case for metallic-dielectric metamaterials [27].

3. Fabrication techniques for MRD metamaterials

3.1. Compacting randomly oriented, jagged-shaped particle distributions

Perhaps the simplest method to fabricate macroscale MRD metamaterials is to compress powder containing a stochastic distribution of particle sizes, shapes and orientations of a dielectric material into pellets. Wheeler et al. [27,44] successfully implemented this technique with SiC particles and a potassium bromide (KBr) host medium as MRD metamaterials. Fig. 2 shows a collection of randomly oriented, jagged SiC particles of different sizes (median size of 0.7 μm) and shapes in a compacted pellet. To understand the magnetic and electric dipole resonances of the inclusions, they first modeled the SiC powder as spheroidal particles with shapes described by the ratio of the half-length of the axes a/b. Orientation-averaged extinction cross-sections C_{ext} normalized by the volume of the spheroids V for various ratio a/b are shown in Fig. 3. Note that the largest dimension of each spheroidal particle is 0.7 μm, corresponding to the median size of the SiC powder. This implies that varying a/b affects not only the shape of an inclusion, but also its size.

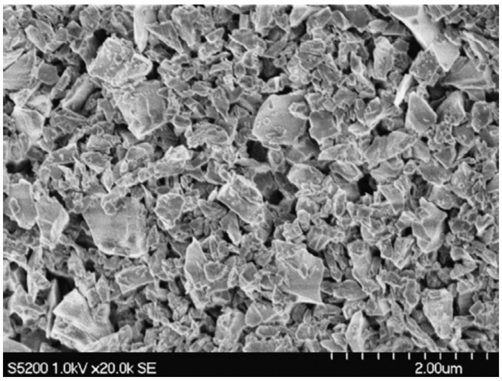

Fig. 2. SEM image of SiC powder sample by Wheeler et al. [27].

The spectral location of the magnetic resonance is essentially unaffected by the particle shape, because the magnetic resonance is a bulk mode that depends on the size of the particle. For spherical inclusions, the frequency of the magnetic dipole resonance can be approximated by $\omega_m \approx \pi c/(|n_s|r_s)$, where $|n_s|$ and r_s are respectively the magnitude of the refractive index and the radius of the sphere [27]. Despite that the inclusion size varies with changing a/b, Wheeler et al. argued that the potential frequency shift caused by varying the size is compensated by rapid changes in $|n_s|$ for the frequency range where the magnetic resonance exists (slightly below the transverse optical phonon frequency of SiC). This explains why the spectral location of the magnetic resonance is nearly unaffected by the ratio a/b. Since only the strength of the magnetic dipole resonance is affected by the particle size, the effective magnetic response of the metamaterial was computed via the Clausius–Mossotti model and by size averaging a distribution of spherical inclusions. Conversely, the electric resonance is induced by a surface mode. As such, the particle shape does affect the electric dipole resonance, because the shape of the particle splits the single sphere resonance into two distinct modes within the frequency band where the real part of the dielectric function of SiC is negative. In order to capture the electric resonance splitting arising in the powder shown in Fig. 2, the effective electric response of the metamaterial was calculated using the Clausius–Mossotti model and by size, shape and orientation averaging a distribution of randomly oriented ellipsoids with three unequal semi-axial lengths a, b and c. Infrared measurements performed on the SiC and KBr pellet, in good agreement with the numerical predictions, showed that the MRD metamaterial exhibits isotropic electric and magnetic resonances in the infrared spectral band.

The spatial arrangement and size distribution of the inclusions, but also fabrication imperfections, undoubtedly affect the effective electromagnetic response of MRD metamaterials. However, Wheeler et al. demonstrate that neither a periodic pattern of inclusions nor spherical inclusions are required to obtain a working MRD metamaterial. In addition, it shows that spherical inclusions are not necessary to obtain an isotropic electromagnetic

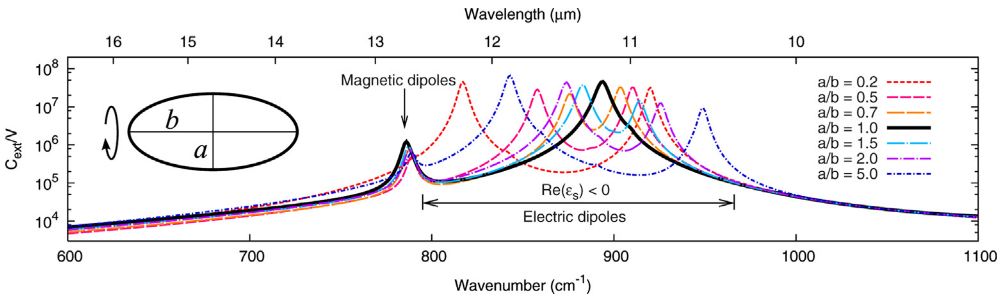

Fig. 3. Orientation-averaged extinction cross-sections of single SiC spheroids in a KBr host medium normalized by its volume [27].

response. It is clear that an individual inclusion in Fig. 2 leads to an anisotropic electromagnetic response. This can be understood by conceptualizing scattering of an electromagnetic wave illuminating a single inclusion in Fig. 2. The fields scattered by an individual inclusion are a strong function of its orientation and only for spherical inclusions scattering is independent of the orientation. However, using a large number of randomly oriented non-symmetric inclusions is equivalent to averaging the scattered fields over all orientations. Thus, an isotropic electromagnetic response is obtained even if the individual inclusions are asymmetric. Finally, the work by Wheeler et al. shows that the shape and size of the inclusions is an adjustable parameter that can be employed to tune metamaterial resonances.

This appears to be the only demonstration where inclusions of a not well-described shape are used, and where a random spatial arrangement of inclusions is employed. While perhaps easier to manufacture, the random collection of compacted particles also presents limitations to the range of possible optical responses that can be obtained, and does not guarantee a uniform concentration of inclusions throughout the host matrix. A direct extension of the compressed pellet MRD metamaterial is to also use the periodicity of the spatial arrangement and the distance between inclusions as parameters for tailoring the optical response of the metamaterial.

3.2. Directed self-assembly

Directed self-assembly could offer a way to create 3D patterns of inclusions in the host medium. Directed self-assembly can be driven by different mechanisms including capillary forces, surface tension and electrostatic forces. Its advantage compared to traditional assembly of microstructures is well documented [58–60]. The ability to simultaneously manipulate, organize, and position a large number of micrometer to nanometer scale components in multiple dimensions enables low-cost, high-throughput manufacturing. Self-assembly can conceivably be used for fabricating optical MRD metamaterials. However, no papers are available in the open literature that document experimental implementation of this manufacturing technique. Petersen et al. [61] proposed a technique, based on the acoustic radiation force associated with a standing pressure wave that enables manipulating micro- and nanoscale particles dispersed in a host fluid. Using three orthogonal piezoelectric transducers, a 3D standing wave pattern can be established in a reservoir containing a dispersed solution of dielectric particles and a liquid polymer host medium. The acoustic radiation force associated with the ultrasound standing wave pattern drives the dispersed particles to the nodes of this pattern, where they accumulate. The 3D standing wave pattern can be designed to match specific geometric MRD metamaterial designs, and the technique is independent of the properties and shape of the inclusions and host medium. The manipulation of micro- and nanoparticles using bulk ultrasound waves has been demonstrated in [62] and is conceptually illustrated in Fig. 4. When the particles have accumulated at the nodes of the standing wave interference pattern, the polymer is crosslinked to fixate the clusters of particles in place, constituting a macroscale optical MRD metamaterial.

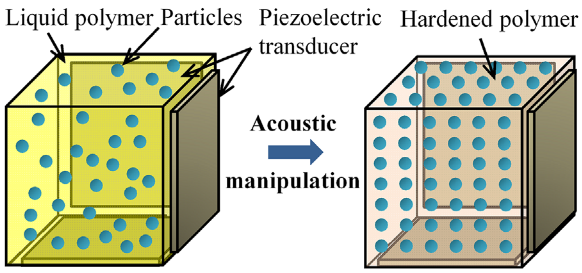

Fig. 4. Directed self-assembly using acoustic standing wave patterns [61].

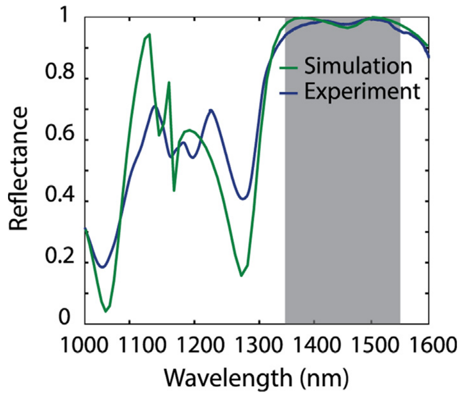

Fig. 5. Reflectance at normal incidence of a metamaterial made of a 2D periodic pattern of Si cylinders of 400 nm diameter and 500 nm height. The lattice spacing is 600 nm [48].

As discussed in Section 3.1, periodicity of the spatial arrangement of inclusions is not required to obtain a working MRD metamaterial, rather it is an adjustable parameter that could be used to control the effective electromagnetic response. Moitra et al. [48] investigated the effect of periodicity of the spatial arrangement of inclusions on the electromagnetic response of a MRD metamaterial. They used cylindrical Si resonators of 400 nm in diameter and 500 nm in height, on a silicon-on-insulator substrate. The objective was to conceive a metamaterial perfect reflector. The authors pointed out that the optical response of the metamaterial should not be a strong function of the periodicity of the spatial arrangement of inclusions because the resonance is isolated within the inclusions. Hence, the absence of coupling between the inclusions should prevent spectral shift of the metamaterial resonance even if the lattice is distorted. This was verified by measuring and computing reflectance at normal incidence for periodic and disordered spatial arrangements of cylinders. Fig. 5 shows spectral distributions of reflectance in the near infrared band for the periodic metamaterial while Fig. 6 displays results for five different levels of disorder.

We observe that the maximum reflectance of the MRD metamaterial decreases as the level of disorder increases. The distribution of separation distances between the cylinders increases with increasing disorder, thus creating a distribution of coupling strengths between the cylinders, which causes a shift in the resonances of the optical response. Moitra et al. argued that near-perfect reflectance from the Si-based MRD metamaterial is not limited to a

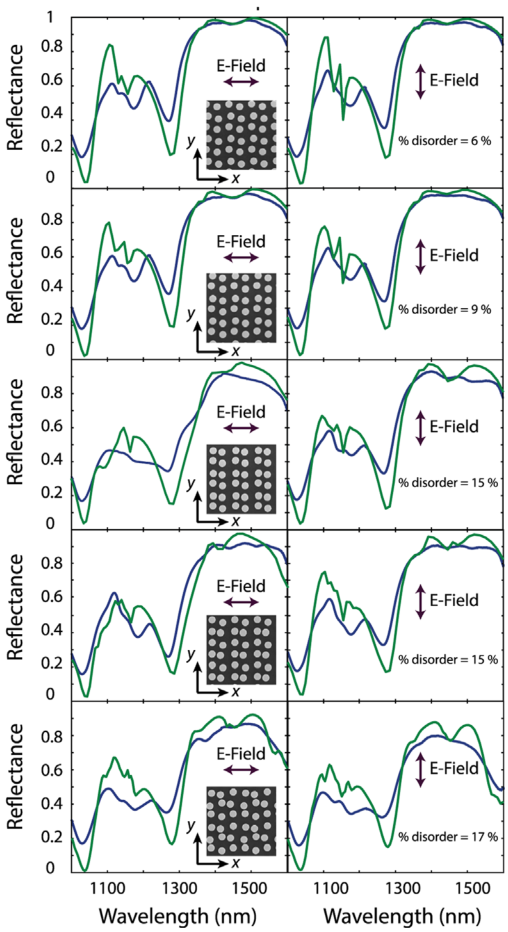

Fig. 6. Reflectance at normal incidence of a metamaterial made of a 2D disordered pattern of Si cylinders of 400 nm diameter and 500 nm height. The panels on the left- and right-hand sides of the figure show the reflectance for an x- and y-polarized incident wave, respectively [48].

periodic spatial arrangement of inclusions as long as the cylindrical resonators are separated by distances large enough to prevent significant inter-inclusion coupling. The compressed pellet technique employed by Wheeler et al. [27] discussed in Section 3.1 cannot prevent inclusions from coming in close proximity to each other. On the other hand, directed self-assembly adds a degree of freedom to MRD metamaterial design and manufacturing by controlling the distance, and thus the coupling, between the inclusions.

The directed self-assembly method based on acoustic waves is significantly different from other fabrication techniques included in this review because it is independent of the material choice, thus lending flexibility to the design of MRD metamaterials. Also, it can be used with spherical inclusions and inclusions of any other shape. Traditional microfabrication techniques, as used for metallic metamaterials, do not offer this flexibility. For instance, microfabrication processes only work for a limited number of materials that can be deposited on silicon wafers, and it is very difficult to reliably fabricate shapes with a curvature in three dimensions, such as spherical shapes. Nevertheless, given that Mie-type resonances are not only achievable in spherical inclusions, microfabrication techniques have been successfully used to implement all-dielectric optical metamaterials. In the next part of this paper, we will review all-dielectric metamaterials that have been implemented using more traditional microfabrication methods.

3.3. *Electron beam lithography*

During the electron beam lithography (EBL) process, a thin layer of a dielectric material is deposited on a dielectric wafer substrate (Fig. 7a) and coated with photoresist (Fig. 7b) prior to exposure to the electron beam that follows the contours of the pattern and features that will be fabricated (Fig. 7c). Developing the resist (Fig. 7d), etching (Fig. 7e), and removing resist (Fig. 7f) completes the fabrication process.

Several publications report on successfully implementing 2D metamaterials using EBL. Zhang et al. [63,64] used EBL in combination with dry etching to fabricate optically active, planar, chiral, dielectric metamaterials consisting of sub-200 nm silicon nitride (Si_3N_4) gammadion features on a fused silica substrate. A chiral metamaterial, however, cannot be categorized as an MRD metamaterial, because the electric and magnetic resonances are not the result of the interaction between an electromagnetic wave and a sub-wavelength resonator such as a cube or a sphere. Nevertheless, all fabrication methods for all-dielectric metamaterials are reported here, as they can potentially be applied to fabricating MRD metamaterials. Levy et al. [65] fabricated a silicon-on-insulator inhomogeneous dielectric metamaterial with feature sizes of approximately 500 nm, covering an area of 10 μm by 22 μm using EBL. Ginn et al. [45] experimentally demonstrated a dielectric MRD metamaterial in the mid-infrared band. Te was first deposited on an optically flat barium fluoride

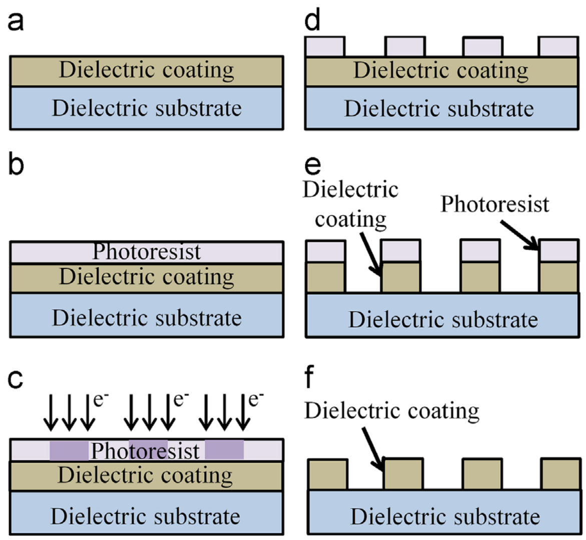

Fig. 7. E-beam lithography fabrication process steps. (a) Deposition of dielectric coating on dielectric substrate, (b) spin coating with photoresist, (c) exposure with e-beam, (d) Photoresist development, (e) etching and (f) photoresist removal.

(BaF_2) substrate using e-beam evaporation. This film was patterned using EBL and etched using reactive ion etching into 1.53 μm Te cubes, covering an area of 1 cm^2 (Fig. 8(a)). The latter implementation covers a 2D macroscale area, but the height of the metamaterial specimen is limited to one layer (one side of the cube, 1.53 μm). Fig. 8(b) shows that the MRD metamaterial fabricated by Ginn et al. exhibits both electric and magnetic resonances in the mid-infrared where the refractive index of Te is large and the losses are small (the measured refractive index of Te by Ginn et al. is $n=5.02+i0.04$ at a wavelength of 10 μm). The authors argue that even if perfect isotropy cannot be achieved with a 2D structured pattern of cubic resonators, their metamaterial achieves a better result than structures based on metallic inclusions such as split-ring resonators. Note that the FOM of the Te-based metamaterial was not reported.

The MRD metamaterial of Moitra et al. [48] discussed in Section 3.2 was fabricated from silicon-on-insulator wafers consisting of a Si substrate and a 500 nm thick crystalline Si film, separated by a 2 μm thick silicon oxide layer (SiO_2). EBL and reactive ion etching were used to fabricate cylindrical resonators in the crystalline Si film resulting in a 2D pattern of cylinders with a diameter of 400 nm and height of 500 nm. Fig. 9 shows a periodic spatial arrangement of these cylindrical resonators. Reflectance as a function of the angle of incidence showed that the electromagnetic response of the MRD metamaterial is anisotropic, although high reflectance was conserved for large angular bands [66]. Staude et al. [46] investigated an MRD metamaterial made of a 2D periodic array of nanosize Si cylinders on a SiO_2 surface using the same fabrication technique as Moitra et al. [48]. The height of the cylinders was fixed at 220 nm throughout their study, while different samples with varying diameters ranging from 400 nm to 600 nm were fabricated. The lattice constant was 800 nm. The cylinders were embedded in SiO_2 using low-pressure chemical vapor deposition (LPCVD). The MRD metamaterial of Staude et al. exhibited near-zero backward scattering in the near infrared spectral band due to spectrally overlapping electric and magnetic resonances, as discussed in Section 2.

Moitra et al. [47,67] experimentally demonstrated a zero-index MRD metamaterial in the near infrared band with nearly isotropic response in transverse magnetic polarization. Fig. 10 displays the structure that consists of 200 μm long alternating Si and SiO_2 rods with a lattice constant of 600 nm. A total of 11 alternating layers of crystalline Si (260 nm thick) and SiO_2 (340 nm thick) were deposited on a 4 in. quartz wafer using LPCVD. A metal etch mask was patterned using EBL, followed by reactive ion etching to form rods. PMMA was then coated onto the

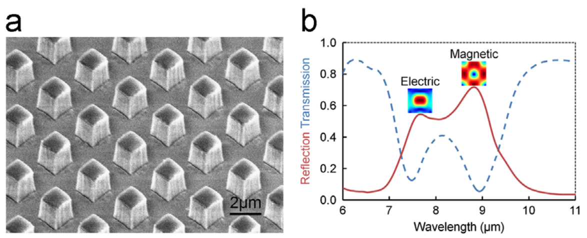

Fig. 8. (a) SEM image of cubic dielectric resonators made of Te coated on a BaF_2 substrate. (b) Measured reflection and transmission showing electric and magnetic resonances at 7.5 μm and 9 μm, respectively [45].

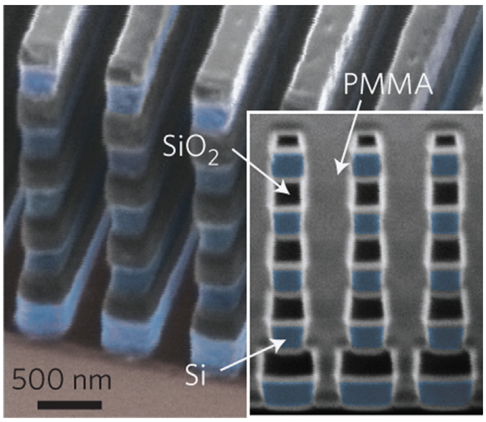

Fig. 10. Ion beam image of the MRD metamaterial of Moitra et al. [47].

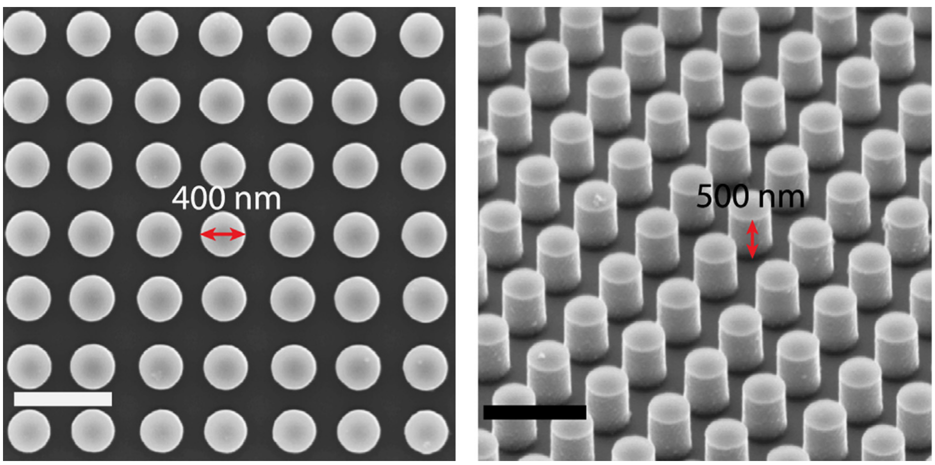

Fig. 9. SEM image of the Si MRD metamaterial of Moitra et al. [48].

sample to fill the air gaps between the rods and create a host medium matching the refractive index of SiO_2.

EBL consumes significant fabrication time because the electron beam traces the contours of all features of the pattern being implemented. As a result, the process is expensive and the metamaterial specimens are limited in size, commonly on the order of 100 μm by 100 μm, with few exceptions [45]. Large-area all dielectric planar chiral metamaterials fabricated by combining several EBL fields with a stitching process were recently demonstrated [64]. A charge dispersion layer was used to solve stitching errors during the serial EBL writing process across different EBL fields. This enables the fabrication of good-quality, large area structures without the limitations normally encountered by stitching errors and field alignment.

The smallest feature size that can be achieved is on the order of tens of nanometers, which is sufficiently small to fabricate functional optical MRD metamaterials. However, EBL is inherently 2D and, thus, a layered structure is needed to expand into the third dimension. This can be achieved by sequentially performing EBL and material deposition. Planarization of the individual layers and alignment accuracy of mating layers may pose a limit to the number of layers that can be deposited on top of each other, when fabricating 3D metamaterials [68]. The fabrication time for one layer is multiplied by the number of layers deposited. As such, the number of layers that can be stacked is also limited by time and cost considerations. Given the 2D nature of the process, and the sequential deposition of layers, the type of inclusions that can be fabricated is limited to cylindrical features. This includes cubes and rods. Spherical inclusions, while theoretically possible if the sphere would be created in several layers, would be difficult to implement.

3.4. Focused ion beam lithography and milling

Focused ion beam (FIB) lithography or focused ion beam milling has become a popular method to fabricate metallic metamaterial prototypes due to its relatively quick processing time compared to EBL, and its ability to create high aspect ratio structures [69]. Individual layers are deposited using e-beam evaporation under high vacuum, ion deposition, or localized chemical vapor deposition [70]. The technique can potentially be used to fabricate MRD metamaterials. For instance, SiC thin films can be deposited on a substrate using plasma-enhanced chemical vapor deposition (PECVD) [71]. Material is then milled by blasting the surface with accelerated Gallium ions [72]. The speed of FIB milling is inversely related to the achieved resolution. To increase the resolution, the beam current must be decreased to maintain the same dosing image, which increases fabrication time. Feature sizes down to 20 nm with lateral dimensions down to approximately 5 nm can be obtained, which is sufficiently small for optical MRD metamaterials. However, the inherent risk with this technique is that removed material may contaminate the finished product, especially when making high aspect ratio structures. Hence, the aspect ratio is limited by re-deposition of the milled material. If a line or hole is milled 10–15 times deeper than its width, re-deposition results in V-shaped cross sections.

Only one publication by Valentine et al. [13] reports using FIB milling to fabricate an all dielectric optical metamaterial consisting of Si and SiO_2 with feature sizes of approximately 110 nm (Fig. 11). Valentine et al. demonstrated cloaking at optical frequencies via the all-dielectric, isotropic and non-resonance based metamaterial shown in Fig. 11. This metamaterial cannot be categorized as an MRD structure, but the fabrication technique could possibly be adapted to fabricate MRD metamaterials. Like EBL, focused ion beam lithography is inherently 2D, requiring stacking several material layers to obtain a 3D structure. Since the FIB milling process is utilized to construct the 2D patterns, alignment between successive layers is less challenging than in the case of EBL. The possible geometrical configurations are limited to 2D patterning.

3.5. Imprinting/embossing techniques

Stamping and embossing techniques are oftentimes used for fabrication of metamaterials. In particular nanoimprint lithography (NIL), shown in Fig. 12, which utilizes a stamp with hard pattern transfer elements

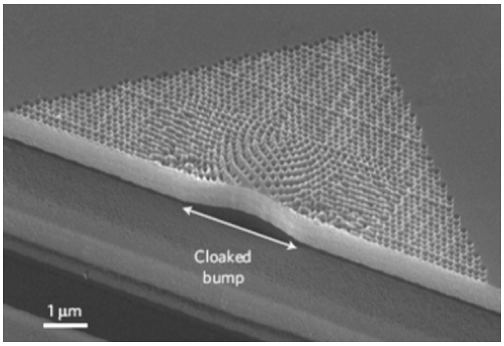

Fig. 11. Scanning electron microscope image of a fabricated carpet cloak by Valentine et al. [13]. The width and depth of the cloaked bump are 3.8 μm and 400 nm, respectively.

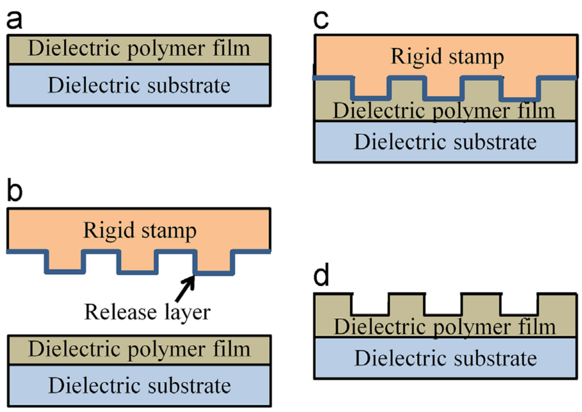

Fig. 12. Nanoimprint lithography fabrication process steps. (a) Deposition of dielectric polymer film on dielectric substrate, (b) heat polymer above its glass temperature, (c) press stamp into polymer film and (d) remove stamp and cool polymer below its glass temperature.

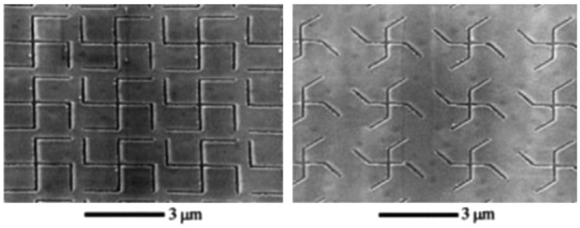

Fig. 13. SEM micrographs of dielectric planar chiral structures fabricated with NIL by Chen et al. [76].

pressed into a polymer layer heated above its glass transition temperature, has been documented to be a viable fabrication method [73–75]. At this temperature, the thermoplastic polymer film becomes a viscous liquid, which can flow and readily take the form of the mold with which it is imprinted. The stamps must be fabricated via another fabrication technique, most commonly EBL and FIB lithography. The resolution of this technique depends on the feasibility of fabricating stamps with small features, the ability of the polymer film to mold to the stamp features with high reliability, the distortion of the features in the transferred pattern, and swelling of the stamp as a result of contact with the polymers [73].

NIL has been utilized to fabricate an all dielectric chiral photonic metamaterial with feature sizes down to 500 nm in hydrogen silsequioxane (HSQ), covering a 3 mm by 3 mm area [76] as shown in Fig. 13. Gammadions were implemented as geometric features. While Fig. 13 does not constitute an MRD metamaterial because of the chiral inclusions, the technique can be used to fabricate MRD structures. The fabrication technique inherently results in tapered sidewalls [77], which could restrict 3D fabrication via layer-by-layer stacking. Throughput rates with NIL are approximately 10^8 times faster than FIB systems [77]. Compared to the earlier listed lithography methods, NIL enables high-resolution, large-scale fabrication in 2D. Stacking of several layers remains necessary to achieve 3D materials, and accurate registration of different layers, subsequently formed with NIL, is difficult to achieve.

4. Discussion and outlook

4.1. Alternative fabrication techniques

Two other fabrication techniques, direct laser writing (DLW) and interference lithography (IL), have been successfully used to manufacture microscale metallic metamaterials, as described in [23]. While not yet demonstrated, these two techniques, in principle, can be adapted to manufacture MRD metamaterials. Fig. 14 schematically illustrates the IL process, which is based on the superposition of two or more coherent optical beams to form a standing wave pattern within a photoresist layer, and follows the same process steps than other lithography techniques, except for the exposure of the photoresist. The ease of making periodic patterns renders this technology a good candidate to fabricate MRD metamaterials. It could also be used to make stacked 3D structures, since the fabrication of one layer happens collectively, i.e., it is not a

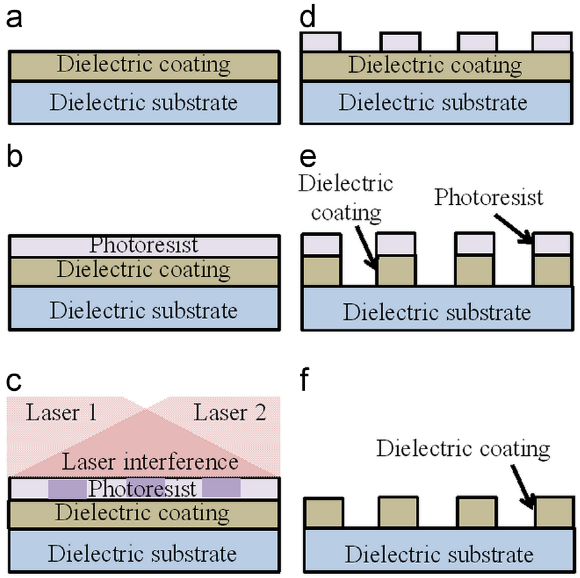

Fig. 14. Interference lithography fabrication process steps. (a) Deposition of dielectric coating on dielectric substrate, (b) spin coating with photoresist, (c) exposure with e-beam, (d) Photoresist development, (e) etching and (f) photoresist removal.

sequential process such as EBL. It has been suggested that interference lithography could be combined with colloidal self-assembly to produce dielectric metamaterials via spin-coating [78]. Direct laser writing (DLW) allows creating 3D structures without layering. However, the thickness is limited to several tens of micrometers. This working range can be extended slightly with dip-in DLW [79]. The focal point of the laser induces a change of solubility in the photoresist. DLW is also sometimes referred to as multi-photon polymerization laser writing. The resolution is typically an order of magnitude larger (100 nm) than EBL, but recent advances in DLW have enabled feature sizes of approximately 50 nm [80,81]. For MRD metamaterials operating at optical frequencies, minimum feature size is not a limitation. As with EBL, the scalability of DLW to fabricating macroscale MRD metamaterials is a major obstacle.

4.2. Outlook

MRD metamaterials could constitute an alternative and possibly a simpler route to realize the implementation of 3D macroscale metamaterials for use in engineering devices. However, only a few publications document experimental proof-of-concept of optical MRD metamaterials or even all-dielectric metamaterials. Fabrication of 3D metamaterials is a challenging problem. While MRD metamaterials consisting of randomly oriented and compressed particles of arbitrary shape have been demonstrated, it is sometimes desirable to create more organized patterns of inclusions to gain better control of the optical response of the MRD metamaterial, as discussed in Section 3.2. Furthermore, one of the main bottlenecks is scaling existing manufacturing techniques that provide

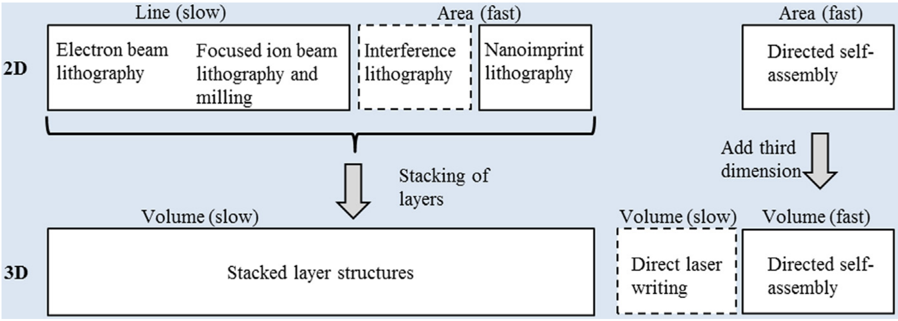

Fig. 15. Overview of optical MRD metamaterial fabrication techniques, showing techniques that have not yet been demonstrated framed with a dashed line.

nanometer or micrometer accuracy and precision while covering macroscale surface areas. Macroscale metamaterials are ultimately desired for implementation in engineering devices. Thus, discrepancy exists between the level of accuracy needed to fabricate the required "meta-atom" features to obtain the desired, tailored, optical response, which is on the nano- or microscale, and the surface (2D) or volume (3D) that needs to be covered to be useful for engineering applications, which is on the macroscale. Furthermore, most microfabrication techniques are well suited for 2D patterning, but expansion into 3D is not straightforward, especially if the out-of-plane dimension must be on the same order of magnitude as the in-plane dimensions. For instance, EBL provides the required precision and accuracy but is a sequential process, i.e., the entire pattern that needs to be fabricated must be traced with the e-beam. While it is theoretically possible to cover large areas with this technique, it would require too much time. Thus, it is primarily useful for proof-of-concept demonstrations. EBL is a 2D technique and expansion into 3D requires subsequent stacking of layers, which is restricted by the registration accuracy of different layers, and the time needed to fabricate the different layers in sequence.

Another 2D technique is NIL, which is more suited for large-scale, low-cost fabrication. A single layer of MRD metamaterial can be created in one fabrication step. Multiple layers can then be deposited on top of each other, but the registration of subsequent layers remains a problem, similar to EBL. While different layers must still be stacked sequentially to fabricate 3D metamaterials, NIL promises to be a viable way to fabricate macroscale optical MRD metamaterials, since these fabrication technique is more scalable in 2D than EBL. Also, these techniques do not allow for fabrication of spherical inclusions, but restrict the MRD metamaterial design to cylindrical inclusions.

No technique is unique to fabricating MRD metamaterials compared to metallic-dielectric metamaterials and, thus, limitations to fabricating macroscale metallic-dielectric metamaterials still apply to fabricating MRD metamaterials. However, the geometric contour of the inclusions in the metamaterial host medium is less complex for MRD than for metallic metamaterials, which relaxes the accuracy and resolution requirement, and reduces the importance of fabrication errors. Nevertheless, from this review, it seems that only a modest reduction in fabrication complexity can be gained from implementing MRD as opposed to metallic metamaterials.

Directed self-assembly offers a completely different approach to MRD metamaterial fabrication and may promise the most viable path to successfully implementing macroscale MRD metamaterials [3]. For instance, the acoustic manipulation technique, based on standing pressure waves, is scalable in three dimensions and is independent of the material properties of the particles. Thus, it could offer scalability, flexibility, and high-throughput. Fig. 15 summarizes the different fabrication techniques discussed in this paper and classifies them as methods that sequentially trace the desired pattern point-by-point and line-by-line and methods that create the desired pattern over an entire area (2D) or volume (3D) at once. Techniques that have not yet been demonstrated but, in principle, can be adapted to fabricated macroscale 3D metamaterials are indicated with a dashed frame.

In conclusion, no experimental demonstration currently exists of macroscale 3D optical MRD metamaterials usable in engineering devices. Several micromanufacturing techniques have been successfully used to fabricate 2D macroscale MRD metamaterials. Extension of these techniques into the third dimension is not trivial, and perhaps the biggest challenge to using micromachining techniques to fabricate true 3D metamaterials. Other techniques such as directed self-assembly could offer an alternative to implementation of macroscale 3D MRD metamaterials. Successful fabrication of these materials would enable myriad engineering applications and could mean a major step forward for the field of metamaterials.

Acknowledgments

This work was partially funded by the National Science Foundation under Grant no. DMR 11-21252. M.F. acknowledges financial support provided by the Army Research Office under Grant no. W911NF-14-1-0210. B.R. acknowledges financial support provided by the Army Research Office under Grant no. W911NF-14-1-0565.

Appendix A. Physics of electric and magnetic resonances in MRD metamaterials

The effective electric permittivity and magnetic permeability of MRD metamaterials can be modeled using the Clausius–Mossotti relations that are applicable when the wavelength in the host medium is much larger than the size of the inclusions and their separation distance [1,44]. In this model, the effective electromagnetic properties are expressed as a function of the polarizabilities of the inclusions [27,44]

$$\frac{\varepsilon_{eff}-\varepsilon_h}{\varepsilon_{eff}+2\varepsilon_h}=\frac{N}{3}\langle\overline{\alpha}_e\rangle \tag{A1.1a}$$

$$\frac{\mu_{eff}-1}{\mu_{eff}+2}=\frac{N}{3}\langle\overline{\alpha}_m\rangle, \tag{A1.1b}$$

where ε_{eff} and μ_{eff} are the effective (relative) permittivity and permeability of the metamaterial, ε_h is the (relative) permittivity of the host medium, N is the number of inclusions per unit volume while α_e and α_m are respectively the electric and magnetic polarizabilities of the inclusions. In Eqs. (A1.1a) and (A1.1b), the brackets indicate averaging of the size of the inclusions while the overline refers to averaging of the shape and orientation of the inclusions [27]. Additionally, since MRD metamaterials are made of dielectric constituents, Eq. (A1.1b) already implies that the (relative) permeability μ_h of the host medium is unity. It is worth noting that when considering the near-field electromagnetic spectrum at a distance smaller than the size of the inclusions or their separation distance, approximating a heterogeneous layer as homogeneous, as done with the Clausius–Mossotti relations, may lead to significant errors [82]. The validity of the effective medium theory for near-field radiative heat transfer predictions was analyzed recently for relatively simple geometries (e.g., layered media) [82–86]. For MRD metamaterials made of inclusions such as spheres or spheroids, the validity of the Clausius–Mossotti relations in the near field of a thermal source could be verified by direct calculation of thermal emission via a discretization-based method [87].

To explain the physical mechanisms responsible for electric and magnetic resonances in MRD metamaterials, spherical inclusions are considered since an analytical solution to Maxwell's equations exist for the case of an isolated sphere (Mie theory). Also, without loss of generality, only a single inclusion size is considered. In the Mie theory, the electromagnetic field scattered by a sphere is expressed as an infinite summation of coefficients a_l^{Mie} and b_l^{Mie} $(1 \le l \le \infty)$ associated with the electric and magnetic fields, respectively, and are given by [26]

$$a_l^{Mie}=\frac{\tilde{m}\psi_l(\tilde{m}X)\psi_l'(X)-\psi_l(X)\psi_l'(\tilde{m}X)}{\tilde{m}\psi_l(\tilde{m}X)\xi_l'(X)-\xi_l(X)\psi_l'(\tilde{m}X)} \tag{A1.2a}$$

$$b_l^{Mie}=\frac{\psi_l(\tilde{m}X)\psi_l'(X)-\tilde{m}\psi_l(X)\psi_l'(\tilde{m}X)}{\psi_l(\tilde{m}X)\xi_l'(X)-\tilde{m}\xi_l(X)\psi_l'(\tilde{m}X)}, \tag{A1.2b}$$

where ψ_l and ξ_l are Ricatti–Bessel functions (prime indicates differentiation with respect to the argument), $\tilde{m}$ is the ratio of refractive index of the sphere, n_s, and the host medium, n_h, while X is the size parameter defined as $2\pi n_s r_s/\lambda_0$, where λ_0 is the free space wavelength and r_s is the radius of the inclusion. For spherical inclusions of uniform size, the electric and magnetic polarizabilities are proportional to the first order Mie coefficients a_1^{Mie} and b_1^{Mie} (dipole terms), and can be written as [44]

$$\langle\overline{\alpha}_e\rangle\equiv\alpha_e=\frac{6\pi i}{k_h^3}a_1^{Mie} \tag{A1.3a}$$

$$\langle\overline{\alpha}_m\rangle\equiv\alpha_m=\frac{6\pi i}{k_h^3}b_1^{Mie} \tag{A1.3b}$$

where k_h is the magnitude of the wave vector in the host medium. Neglecting higher order poles ($l=2, 3,\ldots$) in the effective permittivity and permeability models is physically acceptable if the wavelength is much larger than the size of the inclusions [26].

Both the inclusions and the host medium in MRD metamaterials are non-magnetic, such that tailoring the effective magnetic permeability requires dielectric inclusions with large magnetic dipole resonance (large coefficient b_1^{Mie}). In the long wavelength limit, the magnetic dipole term can be approximated as follows [44]

$$b_1^{Mie}\approx\frac{-2iX^3}{3}\frac{F(\tilde{m}X)-1}{F(\tilde{m}X)+2}, \tag{A1.4}$$

where $F(\tilde{m}X)=2[sin(\tilde{m}X)-\tilde{m}Xcos(\tilde{m}X)]/([(\tilde{m}X)^2-1]sin(\tilde{m}X)+\tilde{m}Xcos(\tilde{m}X))$. The condition for magnetic dipolar resonance can be determined by imposing $b_1^{Mie}\to\infty$, which arises when $F(\tilde{m}X)=-2$ according to Eq. (A1.4). Furthermore, it can be shown that the fundamental resonant wavelength in the host medium normalized by the diameter of the spherical inclusion d is given by [44]

$$\frac{\lambda_h}{d}\approx\tilde{m}. \tag{A1.5}$$

Since it is assumed that the wavelength in the host medium λ_h is much larger than the size of the inclusions d, Eq. (A1.5) reveals that magnetic dipole resonance is achievable when the refractive index (or permittivity) of the spherical inclusion is much larger than the refractive index (or permittivity) of the host medium. For example, if the wavelength is five times larger than the size of the inclusions, magnetic dipole resonance occurs if the refractive index of the sphere is about five, assuming that the host medium refractive index is unity.

Similarly, the electric dipolar resonance of the spherical inclusions, a_1^{Mie}, may induce an effective permittivity less than unity. The electric dipole a_1^{Mie} can be approximated as follows in the long wavelength limit [44]

$$a_1^{Mie}\approx\frac{-2iX^3}{3}\frac{\varepsilon_sF(\tilde{m}X)-\varepsilon_h}{\varepsilon_sF(\tilde{m}X)+2\varepsilon_h}, \tag{A1.6}$$

where ε_s is the relative permittivity of the spherical inclusion. Electric dipolar resonance occurs when $a_1^{Mie}\to\infty$, which is satisfied when (Eq. A1.6)

$$F(\tilde{m}X)=-2\frac{\varepsilon_h}{\varepsilon_s}. \tag{A1.7}$$

Two cases arise from Eq. (A1.7). When $\varepsilon_s\gg\varepsilon_h$ (same condition as for magnetic dipole resonance), $F(\tilde{m}X)\to0$, and electric dipole resonance occurs at a frequency $\omega\approx8.98c_0/n_sd$, where c_0 is the speed of light in vacuum

[44]. This mode is referred to as a bulk electric dipole resonance since the field is confined at the center of the spherical inclusion. Secondly, when the inclusion and host medium permittivities are comparable, i.e., $\varepsilon_s \approx \varepsilon_h$, $|\tilde{m}X| \ll 1$, because the size of the inclusion is assumed much smaller than the wavelength. This results in $F(\tilde{m}X) \to 1$, and the second resonant condition is given by $\varepsilon_s = -2\varepsilon_h$, which is referred to as a surface electric resonance since the fields are more intense at the surface of the spherical inclusion [44]. This electric dipole resonance can be realized when the permittivity of the inclusion is negative, embedded in a host medium with positive permittivity.

Based on this discussion, an effective magnetic response in MRD metamaterials requires inclusions with large permittivity relative to the host medium, while an effective electric response can be achieved via inclusions with large permittivity and/or negative permittivity. At optical frequencies, these requirements are fulfilled via polaritonic materials, which include polar crystals with ionic vibrations (e.g., SiC, quartz, cubic boron nitride) and doped semiconductors with electronic vibrations (e.g., doped Si). As an illustrative example, the real and imaginary parts of the relative permittivity of SiC, ε_s, are shown in Fig. A1.1 [49]. The real part of ε_s takes a very large value in the infrared when the frequency is near the transverse optical phonon frequency of SiC (1.494×10^{14} rad/s). Additionally, the real part of ε_s is negative for frequencies between the transverse and longitudinal (1.825×10^{14} rad/s) optical phonon frequencies. Therefore, it is clear that polaritonic materials like SiC are a good choice for optical MRD metamaterials as they exhibit both large and negative permittivity in the infrared band.

Non-polaritonic materials may also result in MRD metamaterials with electric and magnetic responses at optical frequencies. For instance, Si, which displays low losses and a moderate refractive index (approximately 3.5 in the near infrared band), results in a strong magnetic dipole resonance in the near infrared band. MRD metamaterials made of Si particles with magnetic response in the near infrared band have been discussed in the literature [51]. Other materials such as silica, Ge, Te and TiO_2 display similar behavior [50,52,55].

Despite only considering spherical inclusions for simplicity, the conclusions of this appendix are also applicable to inclusions of other shapes such as cubes and spheroids. As discussed in Section 3, the inclusion shape is a metamaterial adjustable parameter as it affects the strength and spectral locations of the resonances of the inclusions.

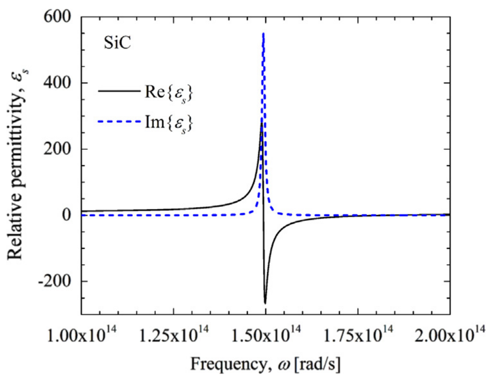

Fig. A1.1. Real and imaginary parts of the relative permittivity of SiC.

References

[1] Cai W, Shalaev V. Optical Metamaterials: Fundamentals and Applications. New York: Springer; 2010.
[2] Solymar L, Shamonina E. Waves in Metamaterials. New York: Oxford University Press; 2009.
[3] Zheludev NI. The road ahead for metamaterials. Science 2010;328:582–3.
[4] Pendry J. Negative refraction makes a perfect lens. Phys Rev Lett 2000;85(18):3966–9.
[5] Smith D, Pendry J, Wiltshire M. Metamaterials and negative refractive index. Science 2004;305:788–92.
[6] Fang N, Lee H, Sun C, Zhang X. Sub-diffraction-limited optical imaging with a silver superlens. Science 2005;308:534–7.
[7] Shalaev V. Optical negative-index metamaterials. Nat Photonics 2007;1:41–8.
[8] Pendry JB, Smith DR. Reversing light: negative refraction. Phys Today 2004:1–8.
[9] Jacob Z, Alekseyev L, Narimanov E. Optical hyperlenses: far-field imaging beyond the diffraction limit. Opt Express 2006;14(18):8247–56.
[10] Liu Z. Lee H. Xiong Y. Sun C. Zhang X. Far-field optical hyperlens magnifying sub-diffraction-limited objects, Science 315, 1686 (2007).
[11] Pendry J, Schurig D, Smith D. Controlling electromagnetic fields. Science 2006;312:1780–2.
[12] Cai W, Chettiar U, Kildishev A, Shalaev V. Optical cloaking with metamaterials. Nat Photonics 2007;1:224–7.
[13] Valentine J, Li J, Zentgraf T, Bartal G, Zhang X. An optical cloak made of dielectrics. Nat Mater 2009;8:568–71.
[14] Engheta N. Circuits with light at nanoscales: optical nanocircuits inspired by metamaterials. Science 2007;317:1698–702.
[15] Liu Z, Boltasseva A, Pedersen R, Bakker R, Kildishev A, Drachev V, et al. Plasmonic nanoantenna arrays for the visible. Metamaterials 2008;2:45–51.
[16] Rephaeli E, Raman A, Fan S. Ultrabroadband photonic structures to achieve high-performance daytime radiative cooling. Nano Lett 2013:1457–61.
[17] Fu C, Zhang M. Thermal radiative properties of metamaterials and other nanostructured materials: a review. Front Energy Power Eng China 2009;3:11–26.
[18] Wang LP, Zhang ZM. Phonon-mediated magnetic polaritons in the infrared region. Opt Express 2011;19:A126–35.
[19] Liu XL, Zhang ZM. Metal-free low-loss negative refraction in the mid-infrared region. Appl Phys Lett 2013;103:103101.
[20] Bai Y, Jiang Y, Liu L. Role of surface plasmon polaritons on the enhancement of the near-field thermal radiation from fishnet metamaterial. J Phys D: Appl Phys 2014;47:445304.
[21] Baxter J, Bian Z, Chen G, Danielson D, Dresselhaus M, Fedorov A, et al. Nanoscale design to enable the revolution in renewable energy. Energy Environ Sci 2009;2:559–88.
[22] Laroche M, Carminati R, Greffet J-J. Near-field thermophotovoltaic energy conversion. J Appl Phys 2006;100:063704-1–10.
[23] Boltasseva A, Shalaev V. Fabrication of optical negative-index metamaterials: recent advances and outlook. Metamaterials 2008;2:1–17.
[24] Zhao Q, Zhou J, Zhang F, Lippens D. Mie resonance-based dielectric metamaterials. Mater Today 2009;12(12):60–9.
[25] Soukoulis CM, Wegener M. Past achievements and future challenges in the development of three-dimensional photonic metamaterials. Nat Photonics 2011;5:523–30.
[26] Bohren C, Huffman D. Absorption and Scattering of Light by Small Particles. Weinheim: Wiley-VCH; 2004.
[27] Wheeler MS, Aitchison JS, Chen JIL, Ozin GA, Mojahedi M. Infrared magnetic response in a random silicon carbide micropowder. Phys Rev B 2009;79:073103.
[28] Lepetit T, Akmansoy E, Ganne J-P. Experimental measurement of negative index in all-dielectric metamaterial. Appl Phys Lett 2009;95:121101-1–3.
[29] Wang J, Xu Z, Xia S, Wang J, Ma H, Qu S. Achieving all-dielectric left-handed metamaterials via single-sized dielectric resonators. J Appl Phys 2012;111:044903-1–5.

[30] Zhao Q, Kang L, Du B, Zhao H, Xie Q, Li B, et al. Isotropic negative permeability composite based on Mie resonance of the BST-MgO dielectric medium. Chin Sci Bull 2008;53(21):3272–6.
[31] Zhao Q, Kang L, Du B, Zhao H, Xie Q, Huang X, et al. Experimental demonstration of isotropic negative permeability in a three-dimensional dielectric composite. Phys Rev Lett 2008;101:027402.
[32] Zhao Q, Du B, Kang L, Zhao H, Xie Q, Li B, et al. Tunable negative permeability in an isotropic dielectric composite. Appl Phys Lett 2008;92:051106.
[33] O'Brien S, Pendry J. Photonic band-gap effects and magnetic activity in dielectric composites. J Phys: Condens Matter 2002;14:4035–44.
[34] Holloway CL, Kuester EF, Baker-Jarvis J, Kabos P. A double negative (DNG) composite medium composed of magnetodielectric spherical particles embedded in a matrix. IEEE Trans Antennas Propag 2003;51(10):2596–603.
[35] Vendik IB, Vendik OG, Gashinova MS. Artificial dielectric medium possessing simultaneously negative permittivity and magnetic permeability. Tech Phys Lett 2006;32(10):30–9.
[36] Kussow A-G, Akyurtlu A, Semichaevsky A, Angkawisittpan N. MgB_2-based negative refraction index metamaterial at visible frequencies: theoretical analysis. Phys Rev B 2007;76:195123.
[37] Yannopapas V. Negative refraction in random photonic alloys of polaritonic and plasmonic microspheres. Phys Rev B 2007;75:035112.
[38] Ahmadi A, Mosallaei H. Physical configuration and performance modeling of all-dielectric metamaterials. Phys Rev B 2008;77:045104.
[39] Qiu C-W, Gao L. Resonant light scattering by small coated nonmagnetic spheres: magnetic resonances, negative refraction, and prediction. J Opt Soc Am B 2008;25(10):1728–37.
[40] Vynck K, Felbacq D, Centeno E, Căbuz AI, Cassagne D, Guizal B. All-dielectric rod-type metamaterials at optical frequencies. Phys Rev Lett 2009;102:133901.
[41] Chern R-L, Liu X-X. Effective parameters and quasi-static resonances for periodic arrays of dielectric spheres. J Opt Soc Am B 2010;27(3):488–96.
[42] Liu LY, Sun JB, Fu XJ, Zhou J, Zhao Q. Artificial magnetic properties of dielectric metamaterials in terms of effective circuit model. Prog Electromagn Res 2011;116:159–70.
[43] Schuller J, Zia R, Taubner T, Brongersma M. Dielectric metamaterials based on electric and magnetic resonances of silicon carbide particles. Phys Rev Lett 2007;99:107401.
[44] Wheeler MS. Ph.D. thesis, University of Toronto, 2010.
[45] Ginn J, Brener I, Peters D, Wendt J, Stevens J, Hines P, et al. Realizing optical magnetism from dielectric metamaterials. Phys Rev Lett 2012;108:097402.
[46] Staude I, Miroshnichenko AE, Decker M, Fofang NT, Liu S, Gonzales E, et al. Tailoring directional scattering through magnetic and electric resonances in subwavelength silicon nanodisks. ACS Nano 2013;7(9):7824–32.
[47] Moitra P, Yang Y, Anderson Z, Kravchenko II, Briggs DP, Valentine J. Realization of an all-dielectric zero-index optical metamaterial. Nat Photonics 2013;7:791–5.
[48] Moitra P, Slovick BA, Yu ZG, Valentine J. Experimental demonstration of a broadband all-dielectric metamaterial perfect reflector. Appl Phys Lett 2014;104:171102.
[49] Palik E. Handbook of Optical Constants of Solids, vol. 1. San Diego: Academic Press; 1998.
[50] Němec H, Kadlec C, Kadlec F, Kužel P, Yahiaoui R, Chung U-C, et al. Resonant magnetic response of TiO_2 microspheres at terahertz frequencies. Appl Phys Lett 2012;100:061117.
[51] Garcia-Etxarri A, Gomez-Media R, Froufe-Perez LS, Opez C, Chandata L, Scheffold F, et al. Strong magnetic response of submicron silicon particles in the infrared. Opt Express 2011;19(6):4815–26.
[52] Geffrin JM, García-Cámara B, Gómez-Medina R, Albella P, Froufe-Pérez LS, Eyraud C, et al. Magnetic and electric coherence in forward- and back-scattered electromagnetic waves by a single dielectric subwavelength sphere. Nat Commun 2012;3:1171.
[53] Garcia-Meca C, Hutardo J, Marti J, Martinez A. Low-loss multilayered metamaterial exhibiting a negative index of refraction at visible wavelengths. Phys Rev Lett 2011;106:067402.
[54] Dolling G, Wegener M, Linden S. Realization of a three-functional-layer negative-index photonic metamaterial. Opt Lett 2007;32:551–3.
[55] Gomez-Media R, Garcia-Camara B, Suarez-Lacalle I, Gonzalez F, Moreno F, Nieto-Vesperinas M, et al. Electric and magnetic dipolar response of germanium nanospheres: interference effects, scattering anisotropy, and optical forces. J Nanophotonics 2011;5:053512.
[56] Wheeler M, Aitchison J, Mojahedi M. Coated nonmagnetic spheres with a negative index of refraction at infrared frequencies. Phys Rev B 2006;79:045105.
[57] Seo B-J, Ueda T, Itoh T, Fetterman H. Isotropic left handed material at optical frequency with dielectric spheres embedded in negative permittivity medium. Appl Phys Lett 2006;88:161122.
[58] Syms RRA, Yeatman EM, Bright VM, Whitesides GW. Surface tension-powered self-assembly of microstructure. J Microelectromech Syst 2003;12(4):387–417.
[59] Srinivasan U, Liepmann D, Howe RT. Microstructure to substrate self-assembly using capillary forces. J Microelectromech Syst 2001;10(1):17–24.
[60] Bohringer KF, Goldberg KY, Cohn MB, Howe RT, Pisano AP. Parallel microassembly using electrostatic force fields. Paper presented at the IEEE international conference on robotics and automation (ICRA). Leuven, Belgium; 1998.
[61] Petersen S, Basu S, Raeymaekers B, Francoeur M. Tuning near-field thermal radiative properties by quantifying sensitivity of Mie resonance-based metamaterials design parameters. J Quant Spectrosc Radiat Transf 2013;129:277–86.
[62] Raeymaekers B, Pantea C, Sinha DN. Manipulation of diamond nanoparticles using bulk acoustic waves. J Appl Phys 2011;109:014317.
[63] Zhang W, Potts A, Bagnall A, Davidson BR. High resolution electron beam lithography for the fabrication of high-density dielectric metamaterials. Thin Solid Films 2007;515:3714–7.
[64] Zhang W, Potts A, Bagnall DM, Davidson BR. Large area all-dielectric planar chiral metamaterials by electron beam lithography. J Vac Sci Technol B 2006;24(3):1455–9.
[65] Levy U, Abashin M, Ikeda K, Krishnamoorthy A, Cunningham J, Fainman Y. Inhomogenous dielectric metamaterials with space-variant polarizability. Phys Rev Lett 2007;98:43901.
[66] Moitra P, Slovick BA, Yu ZG, Valentine J. Supplementary material: experimental demonstration of a broadband all-dielectric metamaterial perfect reflector. Appl Phys Lett 2014;104:171102.
[67] Moitra P, Yang Y, Anderson Z, Kravchenko II, Briggs DP, Valentine J. Supplementary information: realization of an all-dielectric zero-index optical metamaterial. Nat Photonics 2013;7:791–5.
[68] Liu N, Guo H, Fu L, Kaiser S, Schweizer H, Giessen H. Three-dimensional photonic metamaterials at optical frequencies. Nat Mater 2008;7:31–7.
[69] Enkrich C, Perez-Willard F, Gerthsen D, Zhou J, Koschny T, Soukoulis CM, et al. Focused-ion-beam nanofabrication of near infrared magnetic metamaterials. Adv Mater 2005;17:2547–9.
[70] Langford RM, Nellen PM, Gierak J, Fu Y. Focused ion beam micro- and nanoengineering. MRS Bull 2007;32:417–23.
[71] Hsu JM, Tathireddy P, Rieth L, Normann AR, Solzbacher F. Characterization of a-SiCx:H thin films as an encapsulation material for integrated silicon based neural interfaces. Thin Solid Films 2007;516:34–41.
[72] Morita T, Kometani R, Watanabe K, Kanda K, Haruyama Y, Hoshino T, et al. Free-space-wiring fabrication in nano-space by focused-ion-beam chemical vapor deposition. J Vac Sci Technol B 2003;21:2737–42.
[73] Gates BD, Xu Q, Stewart M, Ryan D, Willson CG, Whitesides GM. New approaches to nanofabrication: molding, printing, and other techniques. Chem Rev 2005;105:1171–96.
[74] Chou SY, Krauss PR, Renstrom PJ. Nanoimprint lithography. J Vac Sci Technol B 1996;14(6):4129–33.
[75] Chou SY, Krauss PR, Renstrom PJ. Imprint lithography with 25 nm resolution. Science 1996;272:85–7.
[76] Chen Y, Tao J, Zhao X, Cui Z, Schwanecke AS, Zheludev NI. Nanoimprint lithography for planar chiral photonic metamaterials. Microelectron Eng 2005;78–79:612–7.
[77] Chanda D, Shigeta K, Gupta S, Cain T, Carlson A, Mihi A, et al. Large-area flexible 3D optical negative index metamaterial formed by nanotransfer printing. Nat Nanotechnol 2011;6:402–6.
[78] Xia D, Ku X, Lee SC, Brueck SRJ. Nanostructures and functional materials fabricated by interferometric lithography. Adv Mater 2011;23:147–79.
[79] Bueckmann T, Stenger N, Kadic M, Kaschke J, Froelich T, Kennerknecht C, et al. 3D mechanical metamaterials made by dip-in direct laser writing optical lithography. Adv Mater 2012;24(20):2710–4.
[80] Fischer J, von Freymann G, Wegener M. The materials challenge in diffraction-unlimited direct-laser writing optical lithography. Adv Mater 2010;22:3578–82.
[81] Formanek F, Takeyasu N, Tanaka T, Chiyoda K, Ishikawa A, Kawata S. Three-dimensional fabrication of metallic nanostructures over large

areas by two photon polymerization. Opt Express 2006;14(2):800–9.
[82] Orlov AA, Voroshilov PM, Belov PA, Kivshar YS. Engineered optical nonlocality in nanostructured materials. Phys Rev B 2011;84:045424.
[83] Tschikin M, Biehs S-A, Messina R, Ben-Abdallah P. On the limits of the effective description of hyperbolic materials in the presence of surface waves. J Opt 2013;15:105101.
[84] Guo Y, Cortes CL, Molesky S, Jacob Z. Broadband super-Planckian thermal emission from hyperbolic metamaterials. Appl Phys Lett 2012;101:131106.
[85] Liu XL, Bright TJ, Zhang ZM. Application conditions of effective medium theory in near-field radiative heat transfer between multilayered metamaterials. ASME J Heat Transf 2014;136:092703.
[86] Liu B, Shen S. Broadband near-field radiative thermal emitter/absorber based on hyperbolic metamaterials: direct numerical simulation by the Wiener chaos expansion method. Phys Rev B 2013;87:115403.
[87] Edalatpour S, Francoeur M. The Thermal Discrete Dipole Approximation (T-DDA) for near-field radiative heat transfer simulations in three-dimensional arbitrary geometries. J Quant Spectrosc Radiat Transf 2014;133:364–73.